From Modulators to Biosensing: Silicon Micro-Ring Resonators For Bio-Chemistry Applications

1st Matteo Malagrinò
DEIB
Politecnico di Milano
matteo.malagrino@mail.polimi.it

2nd Riccardo Brizzi
DEIB
Politecnico di Milano
riccardo.brizzi@mail.polimi.it

Abstract

Photonic devices are gaining significant traction in the sensor market due to their ability to detect minute variations in physical parameters with high sensitivity and minimal invasiveness. This work focuses on the experimental characterization of Silicon Micro-Ring Resonators (MRRs) and discusses their utility for biochemical applications. The MRR enables effective molecular detection by exploiting localized changes in the refractive index within the evanescent field when target particles are captured by specific chemical acceptors. The device performance relies on a sophisticated surface functionalization process that integrates photonics, materials science, and biochemistry.

Keywords: Photonic; Silicon Micro-Ring Resonators; Biosensors; Label-Free Molecular Biosensing; Micro-Ring Modulators

I. Introduction

The optical biosensing has emerged as a transformative technology for healthcare, environmental monitoring, and food safety. Compared to traditional analytical methods, such as Enzyme-Linked Immunosorbent Assay (ELISA), photonic sensors offer the advantage of label-free detection, high sensitivity, and the potential for extreme miniaturization. Traditional biochemical assays often require complex labeling steps using fluorescent or radioactive markers, which can be time-consuming, costly, and may alter the natural state of the analyte. To overcome these limitations, Micro-Ring Resonators (MRRs) have been widely adopted as a robust platform for real-time, label-free molecular sensing. The sensing mechanism of an MRR relies on the interaction between the evanescent field of the circulating light and the surrounding medium. When target molecules bind to the resonator's surface, they induce a local change in the refractive index, resulting in a measurable shift in the resonance wavelength ($\Delta\lambda$). In this work, we present an in-depth analysis of a Silicon-on-Insulator (SOI) Micro-Ring Resonator designed for molecular biosensing. We explore the synergy between photonic design and surface chemistry, demonstrating how a tailored functionalization process enables the detection of specific analytes with high sensitivity. The results discussed herein highlight the potential of MRR-based PICs as a scalable and efficient solution for the next generation of Point-of-Care (PoC) diagnostic devices.

II. Silicon Microring Resonators

A. State of the Art

Over the past two decades, Silicon Micro-Ring Resonators (MRRs) have emerged as cornerstone components in integrated photonics, primarily due to their high quality factor (Q), compact footprint, and CMOS compatibility. The versatility of MRRs is evidenced by their dominance in three primary domains: optical modulation, spectral filtering, and sensing. In high-speed communication, MRRs are employed as electro-optic modulators. By integrating $p-i-n$ junctions or using carrier depletion in silicon-on-insulator (SOI) platforms, the refractive index of the ring can be rapidly tuned to shift the resonance peak. Furthermore, the inherent periodic nature of the resonance allows MRRs to function as high-order filters and de-multiplexers in Wavelength Division Multiplexing (WDM) systems, where cascaded configurations achieve box-like filter responses [1]. Perhaps the most transformative application, and the focus of this work, lies in refractive index (RI) sensing. The resonant wavelength (λ_{res}) is highly dependent on the effective index (n_{eff}) of the circulating mode, governed by the relation: $\lambda_{res} = \frac{n_{eff} \cdot L}{m}$, where L is the round-trip length and m is an integer. In the context of biosensing, MRRs offer a label-free platform capable of detecting minute concentrations of analytes. While traditional sensors rely on bulk refractive index changes, state-of-the-art biosensors utilize functionalized surfaces to capture specific biomolecules (e.g., proteins or DNA) directly within the evanescent field of the resonator [2]. Recent advancements have pushed the limits of detection (LoD) toward the single-molecule regime, positioning MRRs as the premier candidate for integrated Point-of-Care (PoC) diagnostic devices, where sensitivity and miniaturization are paramount [3], [4].

III. Experimental Characterization

In this work, we focus on the comparative analysis of the Silicon Micro-Ring (Si-MRR, in Fig.1) by performing an experimental characterization to extract its key operational parameters. The experimental setup (Fig.2) employed a continuous-wave (CW) tunable laser source with an output power set to 0 dBm. Given that Silicon-on-Insulator (SOI) waveguides exhibit high polarization sensitivity, a manual polarization controller was utilized to align the input light to the Transverse Electric (TE) mode. Optical coupling was achieved via single-mode fibers tilted at a 12° angle, targeting the input and through-port grating couplers of the MRR (Fig.3). Fine alignment was maintained using high-precision 3-axis micro-positioners. The transmitted signal was monitored by an optical power meter, revealing an off-resonance baseline power of approximately -22 dBm. This total insertion loss (IL) includes the coupling losses from the two grating couplers—estimated at 6 dB per facet—while the remaining 10 dB is attributed to fiber propagation losses and multiple mating sleeves in the optical path. Following optical alignment, electrical probes were landed on the chip's metal pads to drive the integrated heaters and p-n junctions.

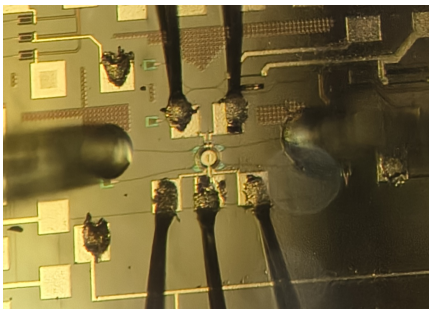

Fig. 1: Microscope detail of the probes on the chip.

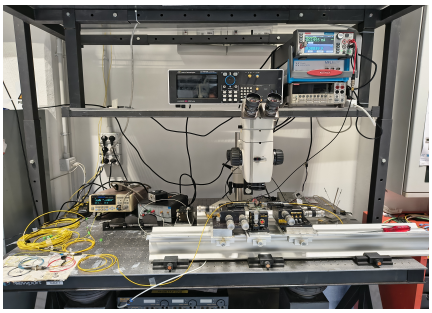

Fig. 2: Overall view of the experimental setup.

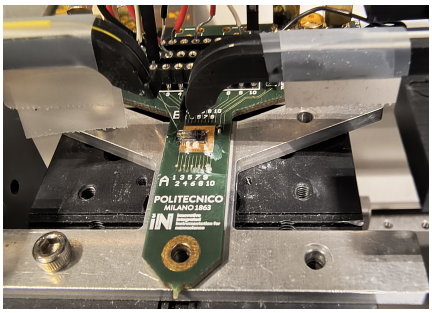

Fig. 3: Detailed view of the Silicon Micro-ring.

A. Spectral Characterization and Data Extraction

The analysis of the transmission spectrum enables the extraction of the resonator's fundamental figures of merit. The *Free Spectral Range* (FSR) and the quality factor Q characterize the resonance periodicity and selectivity, respectively, where $\Delta\lambda_{FWHM}$ denotes the optical bandwidth (BW_{nm}). Furthermore, the modulation depth is quantified by the *Extinction Ratio* (ER).
In this work, resonance tuning and environmental compensation are achieved through the thermo-optic effect. The application of a bias voltage V to the integrated micro-heater induces local Joule heating, resulting in a resonance redshift $\Delta\lambda$. From this shift, the induced optical phase change ($\Delta\phi$) and the effective refractive index variation (Δn_{eff}) are derived, assuming a group index $n_g \approx 4.2$. The system is supposed to operate at a baseline temperature slightly above ambient to allow efficient bi-directional control. The results are summarized below, pairing the optical spectrum with its corresponding physical parameters.

$$
\begin{aligned}
FSR &= \frac{c}{n_g \cdot L_r} \\
Q &= \frac{\lambda_{res}}{BW_{nm}} \\
BW_{GHz} &= \frac{c}{\lambda_{res}^2} BW_{nm} \\
ER_{dB} &= P_{base} - P_{min} \\
\Delta\phi &= 2\pi \frac{\Delta\lambda}{FSR} \\
\Delta n_{eff} &= \frac{\Delta\lambda}{\lambda_{0V}} n_g
\end{aligned}
$$

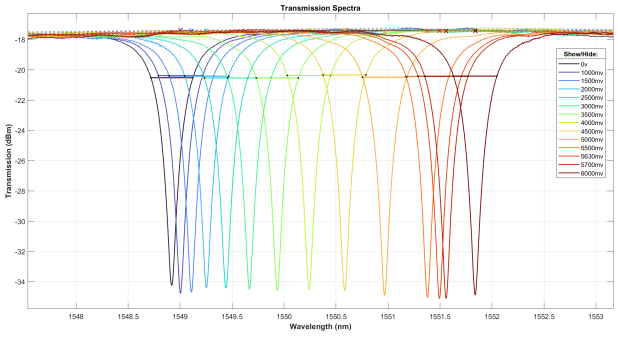

Fig. 4: Transmission of a MRR at various voltage levels.

V (V)	**FSR** (nm)	**BW** (nm)	$\Delta\phi$ (rad)	Δn_{eff} ($\times 10^{-3}$)	**ER** (dB)	**Q** ($\times 10^3$)
0.00	5.131	0.427	0.000	0.00	17.43	3.68
1.00	5.132	0.427	0.099	0.20	17.39	3.68
2.00	5.132	0.428	0.407	0.90	17.37	3.67
3.00	5.133	0.427	0.914	2.00	17.38	3.68
4.00	5.115	0.403	1.624	3.60	16.57	4.30
5.00	5.117	0.417	2.515	5.60	16.90	3.77
5.63	5.118	0.417	3.162	7.00	16.83	3.78
5.70	5.120	0.416	3.239	7.20	16.75	3.79
6.00	5.119	0.415	3.583	7.90	16.75	3.79

TABLE I: Extracted Parameters. ($V_\pi = 5.61$)

B. Geometry Recovery and Dispersion Analysis

The device geometry was validated by back-calculating the cavity length ($L \approx 111.48$ μm) and radius ($R \approx 17.74$ μm) from the experimental FSR at 0 V ($n_g = 4.2$). These results show excellent agreement with the design specifications.

Chromatic dispersion was quantified by evaluating the group index at the spectral extremities, yielding $n_g = 4.1973$ at 1523.7 nm and $n_g = 4.1924$ at 1575.0 nm. The experimental dispersion slope, calculated as $dn_g/d\lambda = \Delta n_g/\Delta\lambda \approx -9.51 \times 10^{-5}$ nm^{-1}, implies a negligible n_g variation (0.0004%) for a typical 0.18 nm sensing shift. This confirms the robustness of the first-order linear model for PoC applications, as second-order effects remain well below the experimental noise floor.

C. Modulation Efficiency and V_π

The modulation efficiency is quantified by the half-wave voltage V_π, representing the bias required for a π phase shift. For the thermo-optic heater, we extracted $V_\pi \approx 5.61$ V, enabling a resonance sweep across more than half the FSR. As shown in Table I, the tuning is non-disruptive: the Q-factor ($\approx 3700 \div 3800$) and Extinction Ratio (> 16.5 dB) remain stable across the entire voltage range, confirming the integrity of the optical cavity during tuning.

IV. Microring Resonators as Biosensors

The transition from an electro-optic modulator to a biosensor relies on the fundamental sensitivity of the guided optical mode to its surrounding environment. While in a modulator the refractive index is perturbed via electrical means (thermal or plasma dispersion), in a biosensor, the perturbation is induced by the presence of biological matter within the reach of the optical field.

A. The Physical Principle: Evanescent Field Interaction and Surface Functionalization

The core physical principle of waveguide-based biosensing is the interaction between the evanescent field and the surrounding medium. When a Transverse Electric (TE) mode propagates through a silicon-on-insulator (SOI) waveguide, the electromagnetic field is not entirely confined within the silicon core ($n_{Si} \approx 3.48$). A fraction of the optical power, known as the evanescent tail (Fig. 5), extends exponentially into the top cladding for approximately 100 to 200 nm: $E(z) = E_0 \cdot \exp(-z/\delta)$, where δ is the penetration depth. In a biosensing configuration, the traditional oxide cladding is locally etched away, and the sensor is exposed to a biological matrix (the complex fluid carrying the molecules of interest, such as blood serum, saliva, or a purified buffer solution). To transition a bare silicon surface from a non-specific transducer to a selective biosensor, a process called bio-functionalization is required. This chemical preparation typically utilizes silane chemistry to attach specific capture agents—such as antibodies, DNA, or proteins—which act as molecular "baits". In this lock-and-key mechanism, these receptors selectively bind only the target analyte, allowing non-target molecules in complex biological matrices to flow past without inducing false-positive shifts [3]. When biological molecules bind to the waveguide surface (Fig. 6), they displace the water-based buffer ($n \approx 1.33$) with denser organic matter (e.g. $n \approx 1.45$). This localized increase in the refractive index modifies the overall effective refractive index (n_{eff}) of the guided mode.

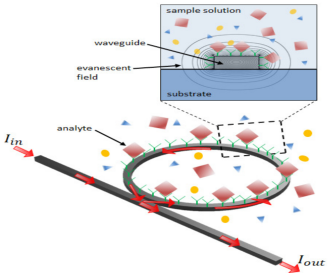

Fig. 5: Illustration of a micro ring resonator with a biochemical layer to attract molecules [5].

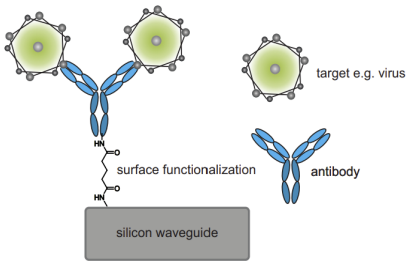

Fig. 6: Surface functionalization demonstrating lock-and-key mechanism [5].

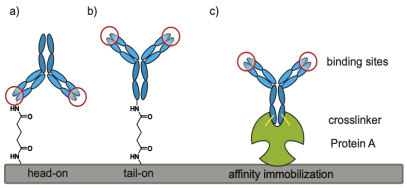

Fig. 7: Head-on (a), tail-on (b) and oriented (c) immobilization with the affinity Protein A [5].

B. Spectral Transduction: The Resonance Shift

The microring acts as an optical transducer, converting this microscopic refractive index change into a macroscopic, measurable optical signal. As target molecules accumulate on the surface, the increase in n_{eff} forces the resonance wavelength (λ_{res}) to increase proportionally to maintain the equation's balance. This results in a red-shift (a displacement toward longer wavelengths) of the transmission notch (Fig. 8): $\Delta\lambda_{res} = \frac{\Delta n_{eff} \cdot \lambda_{res}}{n_g}$ where n_g is the group index extracted during our experimental characterization. By continuously monitoring the position of this spectral dip, the system can track the binding process over time, generating a *binding curve*.

V. Experimental Validation: Performance Limits and Device Viability

To assess the practical utility of the characterized Silicon Microring Resonator (Si-MRR), we developed a predictive sensing model anchored directly to our laboratory results. Unlike standard theoretical studies that rely on idealized Lorentzian curves, this analysis utilizes the actual transmission spectrum at 0 V as a baseline. By mathematically perturbing the experimental data, we demonstrate the sensor's performance in a realistic Point-of-Care (PoC) diagnostic scenario, highlighting where the device excels and identifying its physical operational boundaries.

A. Analytical Performance Metrics and Figure of Merit

Based on the waveguide cross-section (500×220 nm) and the experimentally extracted group index ($n_g \approx 4.2$), we evaluate the following critical parameters:

- **Bulk Sensitivity (S_b):** It quantifies how much the resonance shifts per unit of refractive index change (RIU). It is essential to convert the measured $\Delta\lambda$ (e.g., 0.18 nm) into a concentration value (e.g., mg/dL of glucose).
- **FWHM ($\Delta\lambda_{3dB}$):** Defines the "sharpness" of the notch. In sensing, a narrow FWHM is crucial to distinguish the signal from experimental noise and to track even sub-picometer shifts.
- **Figure of Merit (FOM):** It represents the overall efficiency of the sensor. High sensitivity (S_b) is useless if the peak is too wide (high FWHM); the FOM allows us to compare our device with other state-of-the-art resonators.
- **iLoD / sLoD:** These define the physical and practical limits of the system. They tell us the minimum amount of analyte the sensor can "see" before the signal becomes indistinguishable from noise.

TABLE II: Calculated Biosensing Metrics

Metric	Analytical Formula	Value
S_b	$\frac{\lambda_{res}}{n_g} \cdot f_{clad}$	80 nm/RIU
FWHM	$\Delta\lambda_{3dB}$	0.427 nm
FOM	$\frac{S_b}{FWHM}$	187.35 RIU^{-1}
iLoD	$\frac{FWHM}{S_b}$	$5.34 \cdot 10^{-3}$ RIU
sLoD	$\frac{FWHM}{10 \cdot S_b}$	$5.34 \cdot 10^{-4}$ RIU

The obtained sLoD ($\approx 5.34 \times 10^{-4}$ RIU) is a key result: it proves that our device can resolve refractive index variations typical of clinical glucose fluctuations ($> 10^{-4}$ RIU), confirming its viability for Point-of-Care diagnostics.

B. Clinical Case Study: Macroscopic Glucose Monitoring

We simulated the device's response to physiological glucose concentrations, comparing a healthy fasting state (≈ 90 mg/dL) against a diabetic post-prandial state (≈ 250 mg/dL). Glucose in aqueous solution induces a refractive index variation of $\approx 1.4 \times 10^{-5}$ RIU per mg/dL. A concentration increase of 160 mg/dL produces a measured spectral shift of 0.18 nm. Since this shift (0.18 nm) is significantly larger than the calculated system resolution (0.0427 nm), the device can distinguish these clinical states. This numerical evidence confirms that the characterized Si-MRR is *highly suitable* for robust Point-of-Care (PoC) glucose diagnostics.

C. Active Thermal Stabilization and Operational Bias

A major challenge for silicon-based PoC diagnostics is thermal drift (≈ 80 pm/°C). To neutralize environmental noise, we leverage the integrated micro-heaters characterized in Section III.

1) Thermal Control Logic: The Necessity of a Voltage Bias: To achieve bidirectional thermal control, the micro-heater must be operated at a non-zero Voltage Bias (V_{bias}). This configuration is fundamental for two reasons:

- **Bidirectional Compensation:** By maintaining a baseline bias (e.g., 2.0 V), a feedback loop can counteract ambient cooling by increasing power, or ambient heating by decreasing the bias.
- **Sensitivity Enhancement:** Operating at a bias moves the working point to a region with a higher $d\lambda/dV$ slope, ensuring faster and more precise corrections.

2) Practical Example: Compensating a 0.5 °C Drift: Using our experimental data ($V_\pi \approx 5.61$ V, $FSR \approx 5.13$ nm), we simulated the response to a typical environmental drift of $+0.5$ °C:

1) **Ambient Drift:** A $+0.5$ °C increase induces a red-shift of approximately $+0.040$ nm.
2) **Locked State:** The sensor is initially stabilized at $V_{bias} = 2.00$ V.
3) **Active Restoration:** To counteract the ambient heat, the control loop reduces the heater voltage to 1.87 V. This reduction in local power dissipation perfectly offsets the external thermal gain.

The detection of such a drift (0.040 nm) is made possible by the device's sharp resonance ($FWHM = 0.427$ nm) and high extinction ratio. By employing a Lorentzian tracking algorithm, the system can resolve shifts as small as $1/10$ of the FWHM, effectively translating the statistical data of the entire resonance curve into sub-picometer wavelength precision.

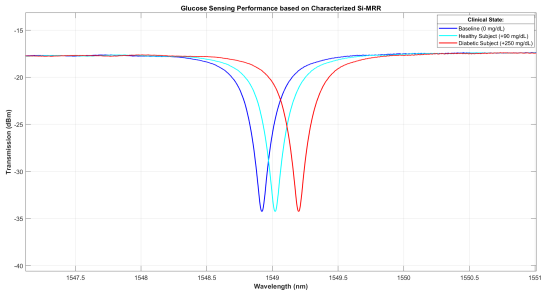

Fig. 8: Simulated biosensing response based on raw experimental data. The high ER ensures robust tracking between the healthy (light blue) and diabetic (red) states.

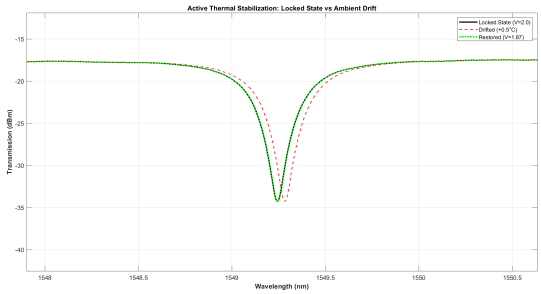

Fig. 9: Active thermal stabilization simulation. The drift induced by a $+0.5$ °C variation (dashed red) is restored to the baseline (dotted green) by modulating the heater voltage.

D. Discussion: Critical Advantages and Physical Limits

The practical viability of the device is assessed by comparing the simulated biological signals with the experimental electro-optic characterization:

Criticality: Without active control, a minimal environmental thermal drift would mask the clinical result. *Advantage:* The high heater efficiency allows the integrated resistors to act as a "thermal buffer", as demonstrated in the previous section.

1) **Dynamic Range vs. Sensitivity:** The large experimental FSR of 5.13 nm allows for a linear response up to concentrations as high as 4500 mg/dL, avoiding "spectral folding".
2) **Signal Integrity in Complex Media:** Our moderate Q-factor (≈ 3680) ensures that the 17.4 dB extinction ratio remains stable, enabling reliable detection in unpurified matrices.

VI. Conclusion

In this work, we experimentally characterized a Silicon Micro-Ring Resonator and validated its performance for biochemical sensing through a predictive numerical model. The device demonstrated a robust Quality Factor of ≈ 3680 and an Extinction Ratio of 17.4 dB, ensuring high signal integrity. The back-calculation of the geometry ($R \approx 17.74$ μm) and the extraction of the dispersion slope ($dn_g/d\lambda \approx -9.51 \times 10^{-5}$ nm^{-1}) confirmed the accuracy of the physical model. Furthermore, we demonstrated that integrated micro-heaters can effectively compensate for environmental thermal drifts, restoring the resonance with sub-picometer precision. These results position the Si-MRR as a reliable and scalable transducer for next-generation, thermally-stabilized Point-of-Care diagnostic platforms.

References

[1] W. Bogaerts *et al.*, "Silicon microring resonators," *Laser & Photonics Reviews*, vol. 6, no. 1, pp. 47–73, 2012.
[2] F. Vollmer and S. Arnold, "Whispering-gallery-mode biosensors," *Nature Methods*, vol. 5, no. 7, pp. 591–596, 2008.
[3] M.-C. Estevez, M. Alvarez, and L. M. Lechuga, "Integrated optical devices for lab-on-a-chip biosensing applications," *Laser & Photonics Reviews*, vol. 6, no. 4, pp. 463–487, 2012.
[4] M. S. Luchansky and R. C. Bailey, "Rapid, multiparametric monitoring of biomarkers and therapeutic agents using silicon photonic microring resonator arrays," *Analytical Chemistry*, vol. 84, no. 2, pp. 793–821, 2012.
[5] P. Steglich et al., "Silicon Photonic Micro-Ring Resonators for Chemical and Biological Sensing: A Tutorial," in IEEE Sensors Journal, vol. 22, no. 11, pp. 10089-10105, 1 June1, 2022, doi: 10.1109/JSEN.2021.3119547.
[6] Katrien De Vos, Irene Bartolozzi, Etienne Schacht, Peter Bienstman, and Roel Baets, "Silicon-on-Insulator microring resonator for sensitive and label-free biosensing," Opt. Express 15, 7610-7615 (2007)
[7] M. S. Luchansky and R. C. Bailey, "High-Q Optical Sensors for Chemical and Biological Analysis," *Analytical Chemistry*, vol. 84, no. 3, pp. 793–821, 2012, doi: 10.1021/ac2029024.
[8] S. Robinson and N. Dhanlaksmi, "Photonic Crystal Based Biosensor for the Detection of Glucose Concentration in Urine," *Photonic Sensors*, vol. 7, no. 1, pp. 11–19, 2017, doi: 10.1007/s13320-016-0347-3.
[9] Diabete.com, "Glicemia: quali sono i valori normali? Valori di riferimento della glicemia o glucosio nel sangue," [Online]. Available: https://www.diabete.com/valori-di-riferimento-della-glicemia/. [Accessed: 14-May-2026].